Long non-coding RNA NMRAL2P promotes glycolysis and reduces ROS in head and neck tumors by interacting with the ENO1 protein and promoting GPX2 transcription

Qian Nie, Huan Cao, JianWang Yang, Tao Liu and BaoShan Wang

Department of Otorhinolaryngology, Second Hospital of Hebei Medical University, Shijiazhuang, China

ABSTRACT

Background. Metabolic reprogramming is a key marker in the occurrence and development of tumors. This process generates more reactive oxygen species (ROS), promoting the development of oxidative stress. To prevent ROS from harming tumor cells, tumor cells can increase the production of reducing agents to counteract excessive ROS. *NMRAL2P* has been shown to promote the production of reductive mRNA and plays an important role in the process of oxidative stress.

Methods. In this study, the clinical data and RNA sequencing of head and neck tumors were obtained from The Cancer Genome Atlas data set. The long non-coding RNA (LncRNA) related to oxidative stress were then identified using differential and correlation analyses. The differential expression and prognosis of the identified lncRNA were then verified using samples from the library of the Second Hospital of Hebei Medical University. Only *NMRAL2P* was substantially expressed in cancer tissues and predicted a poor prognosis. The tumor-promoting impact of *NMRAL2P* was then confirmed using *in vitro* functional assays. The data set was then split into high- and low-expression subgroups based on the median gene expression of *NMRAL2P* to obtain the mRNA that had a large difference between the two groups, and examine the mechanism of *NMRAL2P* on GPX2 using quantitative real-time PCR, RNA binding protein immunoprecipitation assay, and chromatin immunoprecipitation. Mass spectrometry was used to identify *NMRAL2P*-binding proteins and western blotting was used to investigate probable mechanisms.

Results. The lncRNA *NMRAL2P* is associated with oxidative stress in head and neck tumors. *In vitro* functional assays showed that the gene has a cancer-promoting effect, increasing lactic acid and superoxide dismutase production, and reducing the production of ROS and malondialdehyde. *NMRAL2P* promotes the transcription of GPX2 by binding to transcription factor Nrf2. The gene also inhibits the degradation of ENO1, a crucial enzyme in glycolysis, by binding to protein ENO1.

Conclusions. This study shows that *NMRAL2P* can promote glycolysis and reduce the harm to tumor cells caused by ROS. The gene can also be used as a possible target for the treatment of head and neck tumors.

Submitted 25 April 2023
Accepted 29 August 2023
Published 2 October 2023

Corresponding author
BaoShan Wang, hebwangbs@163.com

Academic editor
Yuriy Orlov

Additional Information and Declarations can be found on page 19

DOI **10.7717/peerj.16140**

Subjects Biochemistry, Cell Biology, Molecular Biology, Oncology, Otorhinolaryngology
Keywords *NMRAL2P*, GPX2, ENO1, Glycolysis, ROS

How to cite this article Nie Q, Cao H, Yang JW, Liu T, Wang BS. 2023. Long non-coding RNA NMRAL2P promotes glycolysis and reduces ROS in head and neck tumors by interacting with the ENO1 protein and promoting GPX2 transcription. *PeerJ* **11**:e16140
http://doi.org/10.7717/peerj.16140

INTRODUCTION

The rapid growth of tumors requires considerable energy, and the way the mitochondrial tricarboxylic acid cycle produces ATP cannot keep up with these needs, so glycolysis is the primary way tumors obtain energy (*Hsu & Sabatini, 2008*; *De Berardinis et al., 2008*). Previous studies have also demonstrated that glycolysis is not a unique instance of hypoxia in tumor energy metabolism, but rather that tumors prioritize glycolysis even when there is enough oxygen to create energy for themselves (*Pascale et al., 2020*). Lactic acid is produced in significant quantities during glycolysis, and the acidic environment makes it easier for tumor cell immune escape (*Chen et al., 2022*). Tumor samples show positive changes to glycolysis-related enzymes. For example, the protein levels of GLUT-1, G6PI, LDHA, LDHB, and PFK-L increase, cervical tumor migration increases and the invasion ability of cancer is also enhanced (*Chen et al., 2021*). The RNA expression ratio of PKM2/PKM1 increases, which is an important pathway for colorectal cancer development (*Lan et al., 2020*). Another study showed that the protein expression of GLUT1 in prostate cancer tissue is higher than in adjacent tissues (*Xiao et al., 2018*). Metabolic reprogramming is also a double-edged sword, since glycolysis produces a large number of ROS, which, in the presence of an intracellular oxidant/reductant concentration imbalance, results in the activation of the oxidative stress process, culminating in stress-related DNA and protein damage, and ultimately cell death (*Matsui et al., 2000*; *Park & Chung, 2019*). By controlling the oxidation/reduction balance, tumor cells can proliferate quickly. In order to target tumors and treat cancer, identifying the adjustment point of the tumor is crucial.

Mechanisms such as metabolic reprogramming and oxidative stress trigger abnormalities in cancer tissues that impact numerous lncRNA (*Tan et al., 2021*; *Ginckels & Holvoet, 2022*; *Zhang, Sun & Zhang, 2022*). LncRNA perform a variety of tasks, including altering mRNA transcription by acting on the promoter region of the mRNA. LncRNA can also raise mRNA levels, which are the target of miRNA, by competitive binding with miRNA, and they can serve as a framework for constructed proteins or RNA (*Luo et al., 2020*; *Tian et al., 2020*; *Lin et al., 2020*). LncRNA are promising targets for tumor therapy, but there are currently not enough studies on lncRNA connected to oxidative stress in head and neck tumors.

The differentially expressed lncRNA (DE lncRNA) related to oxidative stress were identified in this study through differential and correlation analyses of the sequencing data of head and neck tumors in The Cancer Genome Atlas data set (TCGA). The DE lncRNA identified were then confirmed using 45 pairs of paired head and neck tumors from the library of the Second Hospital of Hebei Medical University. To further investigate the functional effect of related genes on the migration and invasion of head and neck tumors, human derived head and neck tumor TU177 and human derived head and neck metastatic lesion AMC-HN-8 were selected as cell lines for *in vitro* assays. The influence of lncRNA on carcinogenesis and development was further confirmed by analyzing cell functions and downstream mechanisms.

Table 1 Basic clinical information of patients.

Clinical data ($N = 45$)	
age	62.31 ± 7.80
male	45 (100)
stage	
I	10 (22.22)
II	7 (15.56%)
III	13 (28.89%)
IV	15 (33.33%)
T	
T1	12 (26.67%)
T2	13 (28.89%)
T3	12 (26.67%)
T4	8 (17.78%)
N	
N0	28 (62.22%)
N1	8 (17.78%)
N2	9 (20%)
M	
M0	44 (97.78%)
Mx	1 (2.22%)

MATERIALS AND METHODS

Data acquisition of bulk-sequencing and clinical data

A total of 546 RNA bulk sequencing and clinical data of head and neck tumors (tumor: 502; normal: 44) were downloaded from the GDC website (https/portal.gdc.cancer.gov), and 45 cancer samples and their matching samples (non-tumor tissue adjacent to the cancer) were obtained by the second hospital of Hebei Medical University. Before surgery, the patients did not receive chemotherapy or radiotherapy (clinical information is shown in Table 1). All the samples used in this study are from the biological sample database of the second Hospital of Hebei Medical University. The Research Ethics Committee of Hebei Medical University's Second Hospital approved this study (2021-R012-01). Written, informed consent was obtained from all patients included in this study.

Cell culture and treatment

Head and neck tumor cell lines (TU177, AMC-HN-8) were purchased from Beijing's Beina Chuanglian Institute of Biotechnology. The cell lines were cultured in RPM1640 or DMEM media with 10% fetal bovine serum at 37 °C and 5% CO2. All of the culture medium used in this study were obtained from GIBCO 108 (Gibco, Billings, MT, USA).

Plasmid acquisition, synthesis of antisense oligodeoxynucleotides (ASO)

NMRAL2P overexpression plasmid (NMRAL2P-oe) and pcDNA 3.1 empty plasmid (vector), which was used as the negative control, were both purchased from Sangon

Biotech (Shanghai, China, Sangon). The verification results of NMRAL2P overexpression plasmid are presented in File S1. NMRAL2P-ASO (Antisense oligonucleotide; Ribobio, Guangzhou, China) was designed to knock down the expression of NMRAL2P, and NC-ASO, also provided by RIBOBIO biological company, was used as the negative control. ENO1 and GPX2 were knocked down by cloning the designed target sequence into the vector plasmid pGenesil-1. File S2 presents the sequence of NMRAL2P-ASO, shENO1, and shGPX2 and the sequencing results of shENO1 and shGPX2. ENO1 full-length plasmid (ENO1-FL) and truncated plasmid (ENO1-A, ENO1-B, ENO1-C) with flag tag sequence were purchased from GENEWIZ (Suzhou, China) and the sequencing certificate they provided can be found in File S3.

Total RNA extraction, reverse transcription, quantitative real-time polymerase chain reaction (QRT-PCR)

Total RNA was extracted from the tissues and cells using the EaStep® Super Total RNA extraction kit (LS1040; Promega, Madison, WI, USA). RNA concentration was measured and the quality was assessed using a spectrophotometer (ND-2000; Thermo Fisher, Waltham, MA, USA). The extracted total RNA was reverse transcribed using Roche's Transcriptor First Strand cDNA Synthesis Kit to obtain the cDNA of a tissue or cell, and the GoTaq®qPCR Master Mix (A6001; Promega, Madison, WI, USA) kit was used for QRT-PCR. The data were normalized using the 2-ΔΔCt technique with 18S serving as the internal reference. Table S1 shows the primer sequences used in QRT-PCR.

Nuclear-cytoplasmic separation

Nuclear and cytoplasmic components were separated, and the total RNA of the nucleus and cytoplasm were obtained by NE-PER isolation (78833, Thermo Fisher, California, USA), and then reversed to produce cDNA. The subcellular localization of *NMRAL2P* was examined with QRT-PCR assays using U6 and GAPDH as references.

Cell transfection

TU177 and AMC-HN-8 were cultured in a six-well plate. When the fusion rate reached 80%–90%, 4 μg NMRAL2P-oe/ 5 μg NMRAL2P-ASO and its corresponding negative control (pcDNA3.1, ASO-NC) were combined with 7.5 μg Hieff Trans Liposomal Transfection Reagent (40802ES03; Yeasen Biotechnology, Shanghai, China), and then transferred into TU177 and AMC-HN-8 cells. The transfection efficiency was observed after 48 h, and the cells were collected for further assays.

Cell proliferation assays

After 48 h of transfection, TU177 and AMC-HN-8 cells were digested into cell suspension by trypsin, and then 2*103 (2,000) cells were inoculated into a 96-well plate. To reduce random errors, all experiments were performed in triplicate. After 0 h, 24 h, 48 h and 72 h, 20 μl MTS (G3580; Promega) was introduced into the experimental wells. After being cultured in the incubator for 3 h, Spark®143 multimode microplate reader (Tecan, Männedorf, Switzerland) was used to detect the absorbance of the samples in 490 nm.

Invasion and migration assays

Transwell migration and invasion assays were used to observe the migration and invasion of tumor cells (CLS3396; Corning, New York, USA). Matrigel (CLS354483; Corning) was removed from the −80 °C refrigerator, placed on an ice plate, and then diluted with a serum-free medium at a 1:14 ratio. A precooling gun was used to add 50 μL diluted Matrigel (about 27 μg) to the upper chamber of transwell before placing it in a 37 °C incubator for more than 30 min to ensure that the matrix adhesive was fully solidified. A total of 650 μL of medium containing 10% fetal bovine serum was added to the lower chamber in the migration and invasion assays. Following 48 h of transfection, TU177 and AMC-HN-8 were digested with trypsin, and then 100 μL of serum-free medium, supplemented with 1*105 (100,000) transfected cells, was introduced into the upper chamber. After culturing for 24 h in a 37 °C incubator, the non-invading or non-migrating cells in the upper chamber were carefully removed, and then the chamber was placed in 4% paraformaldehyde and fixed for 30 min, washed with PBS three times, and stained with crystal violet for 30 min. After the crystal violet was removed, washed, and dried, the cells were imaged and then counted in at least three random fields under a microscope.

Cell colony formation assay

TU177 and AMC-HN-8 cells were digested into cell suspension by trypsin 48 h after the migration and invasion assays were performed and 2*103 cells were then planted in a six-well plate. The culture medium was removed from a frosix-well plate after 14 days, the PBS was washed three times, and 4% paraformaldehyde was fixed for 20 min, followed by 20 min of 0.5% crystal violet staining. The number of clones was counted after the crystal violet was removed, washed, and dried. All assays were performed in triplicate.

Measurement of ROS production and lactic acid production

The Lactic Acid Content Assay Kit from Solarbio (Micro method, BC2235; Solarbio, Beijing, China) was used to measure the concentration of lactic acid. The transfected cells were collected, the extract was added, and the supernatant was collected. The cells were then crushed in an ice bath (power: 300W, ultrasonic: 3 s, interval: 7 s, total time: 3 min), and the supernatant was collected after centrifugation. The experimental reagent was then added according to the manufacturer's instructions. The sample's absorbance at 570 nm was detected using Spark® multimode microplate reader, and the concentration of lactic acid was calculated. The Reactive Oxygen Species Assay Kit (CA1410; Solarbio, Beijing, China) was used to measure ROS content. Following transfection, the cell culture medium was taken out and 1 ml of diluted DCFH-DA (2,7-dichlorofluorescein diacetate; reactive oxygen species fluorescent probe) was added. For 20 min, the cells were cultured in a cell incubator at 37 °C. To completely eliminate the DCFH-DA that did not enter the cells, the cells were washed with serum-free cell culture medium three times. The fluorescence intensity before and after stimulation was measured using the excitation wavelength of 488 nm to determine the ROS content.

Measurement of malondialdehyde content and superoxide dismutase activity

The Malondialdehyde (MDA) Content kit (Micromethod, BC0025; Solarbio, Beijing, China) was used to measure MDA content. The transfected cells were collected, the extract was added, and the supernatant was collected. The transfected cells were crushed in an ice bath (power: 200 W, ultrasound: 3 s, interval: 10 s, repeated: 30 times), and the supernatant was collected after centrifugation. The experimental reagent was then added according to the manufacturer's instructions. The absorbance of the sample at 534 nm and 600 nm was then measured using the Spark®143 multimode microplate reader, and the MDA content was calculated. The Superoxide Dismutase Activity Detection Kit (Micro method, BC0175; Solarbio, Beijing, China) was used to detect SOD activity. The supernatant of broken cells was collected and the experimental reagent was added according to the manufacturer's instructions. Finally, the absorbance of the sample at 560 nm was detected using the Spark®143 multimode microplate reader, and the SOD activity was calculated.

RNA binding protein immunoprecipitation assay (RIP)

The PureBinding®RNA Immunoprecipitation Kit was used to perform RIP assays (P0102; Geneseed, Guangzhou, China). TU177 or AMC-HN-8 cells were seeded in a 10-cm dish at 70%–80% confluence, harvested by trypsinization, and lysed with RIP cell lysate. The cell lysates were added to the target protein antibody or the magnetic bead coupling complex of Anti-Rabbit IgG, respectively, and incubated overnight at 4 °C. The precipitated RNA from each group was extracted *via* washing, adsorption, and purification, and the cDNA was subsequently obtained using reverse transcription. The relevant verification experiments were then carried out using QRT-PCR. All the experiments were repeated, independently, three times.

Chromatin Immunoprecipitation Assay (ChIP)

The EZ-Magna ChIP®A/G Chromatin Immunoprecipitation Kit (17-10086; Millipore, Burlington, MA, USA) was used to perform ChIP assays. TU177 cells were seeded in a 10-cm dish, then transferred into NMRAL2P-oe and the vector. After 48 h, the cells were collected with trypsin, and then formaldehyde was cross-linked for 10 min. Next, the lysate and ultrasonic treatment were added to an average size of 300–500 base pairs and then fixed with Nrf2 antibody (80593-1-RR; Proteintech, Wuhan, China) magnetic beads complex to form a protein-DNA complex. The DNA from the sample was then washed out of the complex, and then the DNA was verified through ChIP-QPCR. All the experiments were repeated, independently, three times.

MS2-12X-dependent RNA pull-down assay

We used BamHI and EcoR I to digest MS2-12X and NMRAL2P-oe. Gel electrophoresis was used to check whether the digestion was successful, and the plasmids and fragments were recovered. The 12X fragment was ligated with NMEAL2P-oe with T 4 ligase, and sequencing was used to check whether the connection is successful. The corresponding sequencing results are shown in File S2. Finally, the NMRAL2P-oe plasmid and PSL-MS2 plasmid with 12X sequence were simultaneously transferred into TU177 cells at a 1:1 ratio,

and then the proteins of the GFP antibody group and negative control lgG antibody group were collected with a RIP assay and then analyzed using mass spectrometry.

Mass spectrometry was performed using the methods described by *Chen et al. (2019)*: the protein used for mass spectrometry was hydrolyzed by FASP, and then the peptide mixture was loaded on a reverse phase trap column (Thermo Fisher Scientific Acclaim PepMap100, 100 μm*2 cm, nanoViper C18) and connected to a C18-reversed phase analytical column (Thermo Fisher Scientific Easy Column, 10 cm long, 75 μm inner diameter, 3 μm resin; Thermo Fisher Scientific, Waltham, MA, USA) in buffer A (0.1% formic acid) and separated with a linear gradient of buffer B (84% acetonitrile and 0.1% formic acid; flow rate was 300 nL/min). After separation, the samples were analyzed by LC-MS/MS on a Q Exactive mass spectrometer (Thermo Science Fisher Scientific). The LC-MS/MS spectrum and MS/MS spectra were analyzed using the MASCOT engine (Matrix Science, UK, Version 2.2). The following settings were used for protein identification: peptide mass tolerance = 20 ppm, MS/MS tolerance = 0.1 Da, enzyme = trypsin, missed cleavage = 2, fixed modification: Carbamidomethyl (C), and variable modification: oxidation (M).

Western blot

Following 48 h of transfection, 200 μL of lysate was added to the six-well plate (RIPA lysate: R0010; Solarbio, Beijing, China; PMSF: P0100; Solarbio, Beijing, China; protease inhibitor: G6521, Promega, Madison, WI, USA; using a 100:1:1 ratio). The cell protein lysate was mixed with protein sample loading buffer (LT103; Epizyme, Shanghai, China) at a 4:1 ratio, and then boiled for 5 min at 95 °C in a metal bath. An identical volume of (25 μg) protein was added to the 10% sodium dodecyl sulfate-polyacrylamide gel electrophoresis plate (SDS-PAGE) for electrophoresis. The protein was then transferred to the polyvinylidene fluoride membrane. The membrane was sealed with 5% bovine serum albumin for 2 h and then incubated with corresponding primary antibodies at 4 °C overnight. The sample was rinsed with TBST the next day and then incubated with the corresponding secondary antibody at ambient temperature for 2 h. Chemiluminescence was displayed using Fluorescent XRS+ (Bio-Rad, Hercules, CA, USA). β-actin served as the internal reference, the first antibody was anti-ENO1 (1:1000, ET1705-56; Huabio, Hangzhou, China) and anti- β actin (1:10000; 81115-1-RR; Proteintech, Wuhan, China). The second antibody was Anti-Rabbit IgG (Haul) (1:10000, SA00001-2; Proteintech, Wuhan, China)

Statistical analysis

SPSS (version 16.0; Chicago, IL, USA) and R were used for the statistical analysis (version 4.1.2; *R Core Team, 2021*). Graphs were generated with GraphPad Prism software (version 7.0; GraphPad Inc., San Diego, CA, USA). *T*-test was used to assess the differences between groups of numerical variables with normal distribution, and the rank sum test was employed if the numerical variable deviated from the normal distribution. The proliferation curve was statistically analyzed by two-way ANOVA. The classified variables were the chi-square test or Fisher exact probability method, and a Kaplan–Meier analysis was used for a survival analysis.

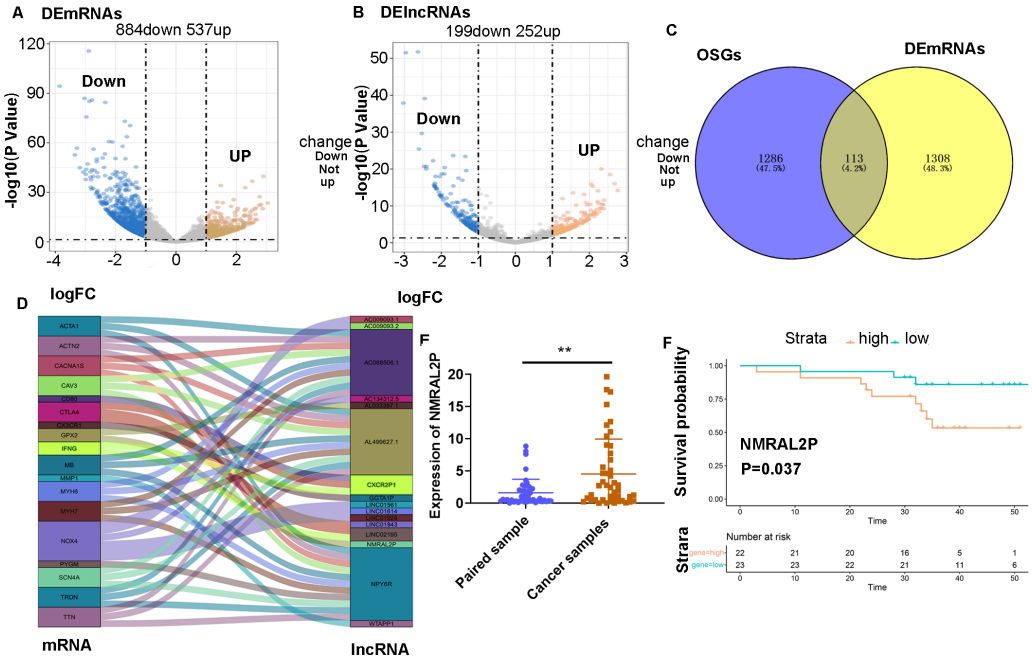

Figure 1 Screening of lncRNA related to oxidative stress. (A) Differential analysis of mRNA expression in head and neck tumor samples. (B) Differential analysis of lncRNA expression in head and neck tumor samples. (C) Oxidative stress-related mRNA. (D) Oxidative stress-related lncRNA. (E) Differential expression of *NMRAL2P* in 45 pairs of clinical samples. (F) Prognostic analysis of *NMRAL2P* in 45 pairs of clinical samples.

Full-size DOI: 10.7717/peerj.16140/fig-1

RESULT

Identifying the lncRNA involved in regulating oxidative stress

RNA-seq and clinical data of 546 head and neck tumors were obtained from TCGA, including 502 tumor samples and 44 normal samples. The "limma" package was used to analyze the differentially expressed mRNA (DE mRNA) and DE lncRNA between the normal samples and cancer samples. A total of 1,421 DE mRNA were obtained through the differential analysis, of which 537 were upregulated and 884 were downregulated in head and neck tumors (Fig. 1A). A total of 451 DE lncRNA were obtained, including 252 upregulated lncRNA and 199 downregulated lncRNA (Fig. 1B). A total of 1,399 mRNA associated with oxidative stress were retrieved from Genecards (Table S2), of which 113 were differentially expressed in head and neck tumor samples (Fig. 1C).

A Pearson correlation analysis was then performed between the 113 DE mRNA related to oxidative stress and 451 DE lncRNA, and 16 DE lncRNA associated with oxidative stress were screened (correlation coefficient > 0.7 and *P* Value < 0.001; Fig. 1D).

NMRAL2P was differentially expressed in 45 pairs of samples and was associated with poor prognosis

A total of 45 pairs of head and neck samples from the Second Hospital of Hebei Medical University were used as the verification set to confirm the differential expression of the 16 identified DE lncRNA to screen those associated with oxidative stress. Only *NMRAL2P* was

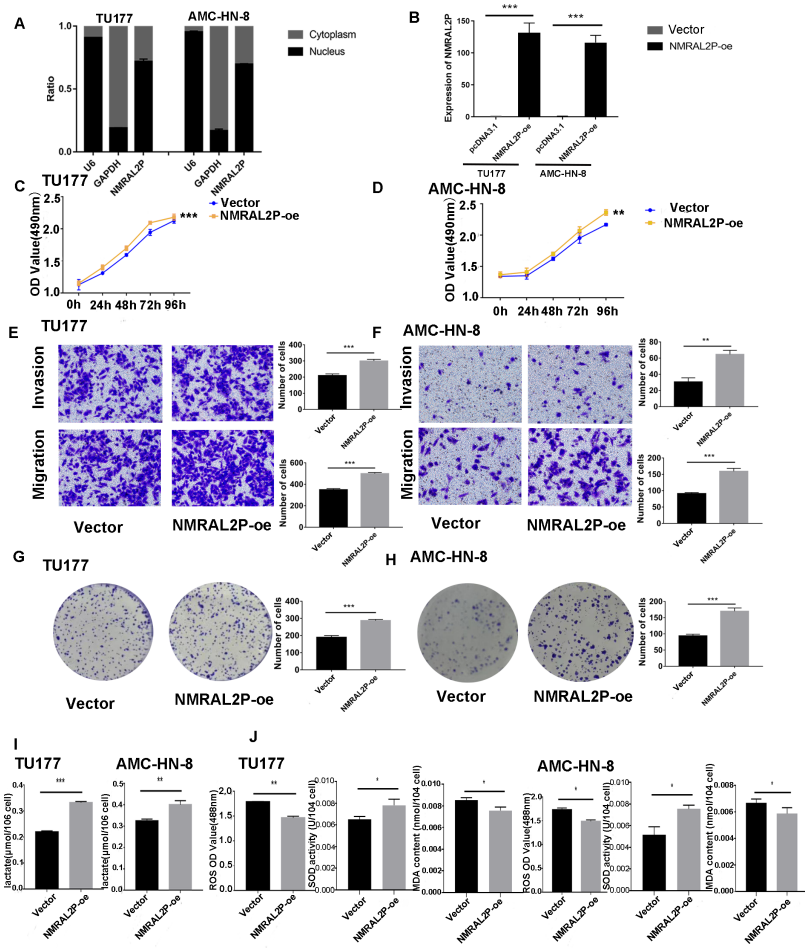

Figure 2 Functional assays of *NMRAL2P* overexpression. (A) Subcellular localization of *NMRAL2P* in cancer cells. (B) Verification of *NMRAL2P*-oe overexpression efficiency in TU177 and AMC-HN-8 cells by QRT-PCR. (C–D) Changes in TU177 and AMC-HN-8 cell viability after being transfected with *NMRAL2P*-oe, verified by MTS assay. (E–F) Changes in cell migration and invasion ability of TU177 and AMC-HN-8 after being transfected with *NMRAL2P-oe*, verified by Transwell assay. (G–H) Changes in proliferation activity of TU177 and AMC-HN-8 after being transfected with *NMRAL2P*-oe, verified by clone formation assay. (I–J) Changes in lactic acid level, ROS yield, SOD activity and MAD content of TU177 and AMC-HN-8 after being transfected with *NMRAL2P*- oe. (ROS, Reactive Oxygen Species; SOD, Superoxide Dismutase; MAD, Malondialdehyde; NMRAL2P-oe, Overexpression of NMRAL2P Vector:pcDNA3.1).

Full-size DOI: 10.7717/peerj.16140/fig-2

highly expressed in head and neck tumors (Fig. 1E) and high expression of the gene was associated with poor prognosis (Fig. 1F). Subcellular localization showed that *NMRAL2P* is mainly located in the nucleus, accounting for approximately 60% of the total *NMRAL2P* found in the cell (Fig. 2A).

NMRAL2P affects the migration, invasion, and proliferation of head and neck tumor cells *in vitro*

NMRAL2P-oe was transferred into TU177 and AMC-HN-8 cells, respectively, to further study the impact of *NMRAL2P* on the function of head and neck tumor cells. The

overexpression of *NMRAL2P*-oe was verified using QRT-PCR. Compared with the control group, the expression of *NMRAL2P* increased around 100x in the overexpression group (Fig. 2B), and compared to the vector, the *NMRAL2P* overexpression increased the viability, migration, invasion, and proliferation of tumor cells (Figs. 2C–2H). To reverse-verify the function of *NMRAL2P* in head and neck tumor cells, we transferred *NMRAL2P*-ASO into TU177 and AMC-HN-8 cells, respectively, and the relative expression of *NMRAL2P* in TU177 and AMC-HN-8 was knocked down by more than 40% (Figs. 3A, 3B). The knockout efficiency of *NMRAL2P*-ASO met the requirements for functional assays. During the assays, it was observed that the survival, migration, invasion, and proliferation of cells in the knockdown group were substantially poorer than that of the negative control group (NC; Figs. 3C–3H), verifying that the expression of *NMRAL2P* improves the viability, migration, invasion, and proliferation of head and neck tumor cells.

NMRAL2P affects the production of lactic acid, ROS, SOD, and MDA

To further investigate whether *NMRAL2P* influences oxidative stress and glycolysis-related processes, we transferred *NMRAL2P*-oe and *NMRAL2P*-ASO into TU177 and AMC-HN-8 cells using the same experimental methods used previously, and measured lactic acid, SOD, MDA, and ROS using a micromethod and fluorescence probe. Increased expression of *NMRAL2P* led to an increase in lactic acid and SOD. Conversely, ROS and MDA in cells were negatively correlated with *NMRAL2P* expression, meaning ROS and MDA decreased as *NMRAL2P* expression increased (Figs. 2I, 2J). When *NMRAL2P* was knocked down, the opposite results were observed (Figs. 3I, 3J). These results indicate that *NMRAL2P* may promote the production of lactic acid and SOD and inhibit the production of ROS and MDA, suggesting that *NMRAL2P* can enhance glycolysis and reduce oxidative stress.

NMRAL2P binds to ENO1 and enhances its stability

In order to further investigate the mechanism of *NMRAL2P*, the 12X sequence was introduced into the GFP vector together with the *NMRAL2P* sequence (Fig. 4A). The protein was then brought down using the GFP vector and the lgG antibody for the mass spectrometry (MS) analysis (File S4). ENO1 was chosen for additional analysis based on the MS results since it is a crucial enzyme in glycolysis. RIP assays were carried out in TU177 and AMC-HN-8 using the ENO1 antibody and the lgG antibody as a negative control. *NMRAL2P* was enriched in the ENO1 antibody group and was around 20 times greater than in the lgG group (Fig. 4B). To investigate the precise site of *NMRAL2P* binding to protein ENO1, a truncated plasmid tagged ENO1 with a flag tag was used to divide ENO1 into three segments: ENO1-A (1-97aa), ENO1-B (97-237aa), and ENO1-C. (237-434aa). ENO1 truncation efficiency was verified using western blot (Fig. S1). RIP experiment results showed that NMRAL2P is mainly enriched in the ENO1-C group (Fig. 4C). *NMRAL2P*-oe and *NMRAL2P*-ASO and their corresponding vectors were then transferred into TU177 and AMC-HN-8 cells, respectively, and the difference in ENO1 protein content was analyzed. Upregulated *NMRAL2P* raised ENO1 protein content compared with the vector, and downregulated *NMRAL2P* lowered ENO1 protein content compared with NC (Figs. 4D, 4E). To verify the results of previous studies that reported that RNA affects the protein

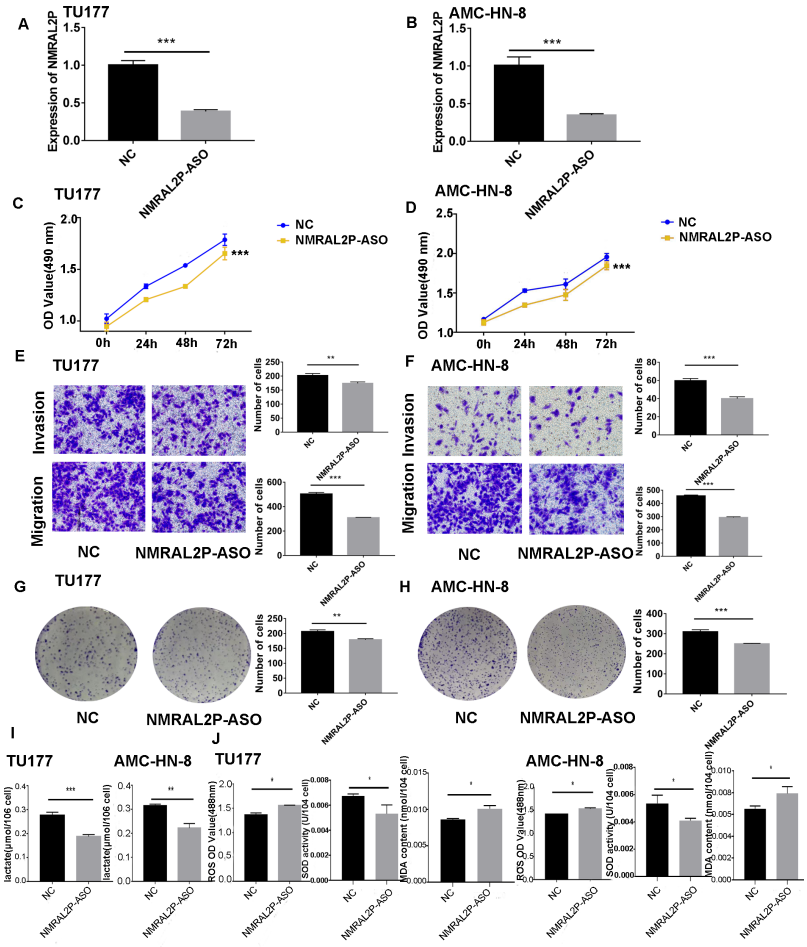

Figure 3 **The functional assay of *NMRAL2P* knockdown.** (A–B) Verification of *NMRAL2P*-ASO knockdown efficiency in TU177 and AMC-HN-8 cells by QRT-PCR. (C–D) Changes in cell viability of TU177 and AMC-HN-8 after being transfected with *NMRAL2P*-ASO, verified by MTS assay. (E–F) Changes in cell migration and invasion ability of TU177 and AMC-HN-8 after being transfected with *NMRAL2P*- ASO, verified by Transwell assay. (G–H) Changes in proliferation activity of TU177 and AMC-HN-8 after being transfected with *NMRAL2P*-ASO, verified by clone formation assay. (I–J) Changes in lactic acid level, ROS yield, SOD activity and MAD content of TU177 and AMC-HN-8 after being transfected with *NMRAL2P*- ASO. (ASO, Antisense oligonucleotide; NC, NC-ASO, Negative control of NMRAL2P knockdown; NMRAL2P-ASO, Knocks down the expression of NMRAL2P; QRT-PCR, quantitative real time polymerase chain reaction).

Full-size DOI: 10.7717/peerj.16140/fig-3

content by affecting protein degradation, *NMRAL2P*-oe and *NMRAL2P*-ASO and their vectors were transferred into TU177 and AMC-HN-8, respectively, and cycloheximide was added to block protein synthesis. Proteins were collected at 0 h, 3 h, 6 h, 9 h, and 12 h and western blot was used to detect the protein level of ENO1. ENO1 was found to be more stable in the *NMRAL2P* overexpression group, whereas its half-life was reduced in the gene downregulation group (Figs. 4F–4G). The protein level of ENO1 in cells without cycloheximide did not decrease significantly after 12 h (Fig. S2). These results indicated that *NMRAL2P* can attach to ENO1 and aid in ENO1's protein stability.

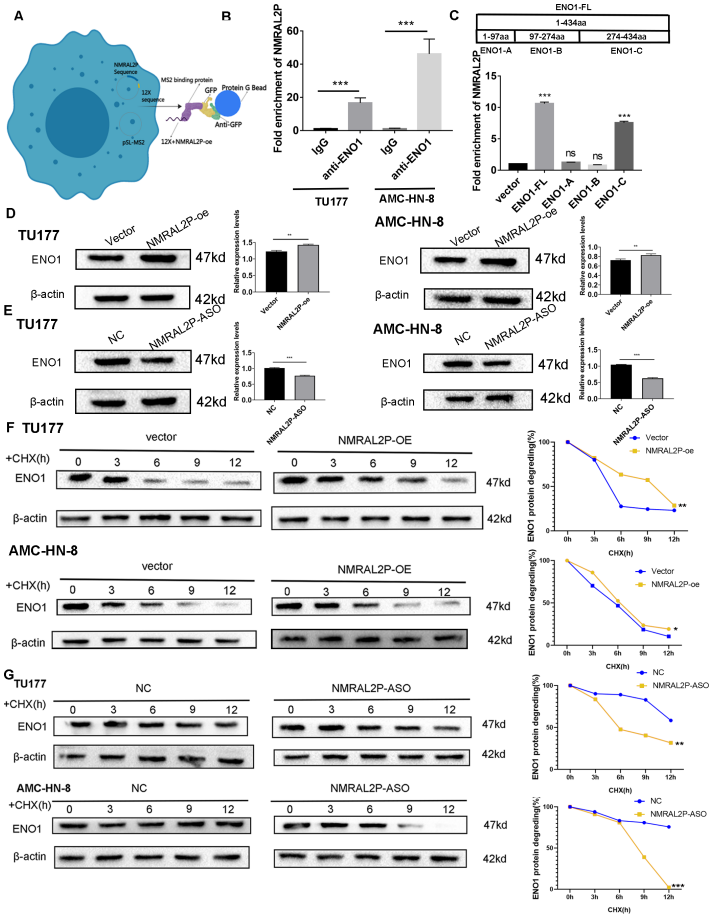

Figure 4 ***NMRAL2P*** **combined with ENO1 to delay the degradation of ENO1.** (A) MS2-12x pulldown process. (B) The binding of ENO1 and *NMRAL2P* was verified by RIP assay (with lgG antibody as the negative control). (C) The full-length plasmid ENO1 with flag tag (ENO1-FL) and truncated plasmid (ENO1-A, ENO1-B, ENO1-C) were transfected into TU177 cells for the RIP assay, and QRT-PCR was used to detect the enrichment of *NMRAL2P*. (D–E) Western blot was used to verify the changes of ENO1 after *NMRAL2P*-oe and *NMRAL2P*-ASO transfection in TU177 and AMC-HN-8 cells. (F–G) Comparing the degradation of ENO1 after *NMRAL2P*-oe and *NMRAL2P*-ASO were transferred into TU177 and AMC-HN-8 cells (with Vector, ASO-NC as negative control) by Western blot assay. (RIP, RNA Binding Protein Immunoprecipitation; NC, NC-ASO, Negative control of NMRAL2P knockdown; Vector: pcDNA3.1; CHX, Cycloheximide).

Full-size DOI: 10.7717/peerj.16140/fig-4

NMRAL2P acts on ENO1 for tumor promotion

We transferred the ENO1 knockdown plasmid and used QRT-PCR and western blot to confirm knockdown effectiveness. In TU177 and AMC-HN-8 cells, the levels of ENO1 mRNA were reduced by more than 40% and the protein level of ENO1 in the shENO1 group was significantly lower than in the vector (pGenesil-1) group (Figs. 5A, 5B). After knocking down the levels of ENO1 mRNA, the migration, invasion, and proliferation abilities of tumor cells decreased (Fig. S3). Functional recovery assays were carried out to further clarify the role of *NMRAL2P* and ENO1 in tumor promotion. MTS, Transwell, and clone formation assays showed that *NMRAL2P* overexpression increased the viability,

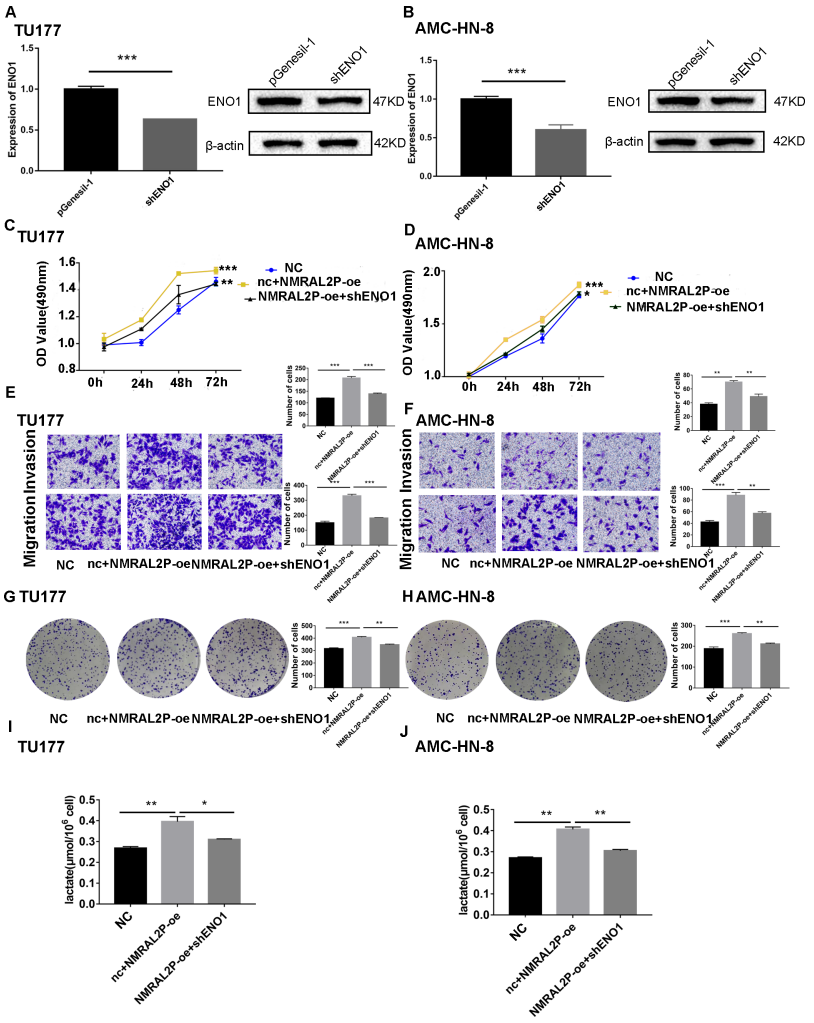

Figure 5 ***NMRAL2P* plays a role in promoting cancer through ENO1.** (A–B) Verification of shENO1 knockdown efficiency in TU177 and AMC-HN-8 cells by QRT-PCR and western blot. (C–H) MTS, Transwell, and colony formation demonstrated that knockdown of ENO1 partially attenuated the enhanced cell proliferation, migration, and invasion induced by overexpression of *NMRAL2P* in TU177 and AMC-HN-8 cells. (I–J) Knockdown of ENO1 partially attenuated the enhanced lactic acid yield induced by overexpression of *NMRAL2P* in TU177 and AMC-HN-8 cells. (NC: pcDNA3.1 + pGenesil-1, nc + NMRAL2P-oe: pGenesil-1 + NMRAL2P-oe).

Full-size DOI: 10.7717/peerj.16140/fig-5

migration, invasion and proliferation of tumor cells, while ENO1 gene knockout partially counteracted this tumor promoting effect (Figs. 5C–5H). The overexpression of *NMRAL2P* led to an increase in lactic acid synthesis, and the downregulation of ENO1 led to a decrease in lactic acid production (Figs. 5I–5J), indicating that *NMRAL2P* acts on ENO1 to promote head and neck tumor cells.

NMRAL2P promotes GPX2 transcription through Nrf2

Patients with head and neck tumors in the TCGA data set were divided into high- and low- expression groups according to the median expression of *NMRAL2P*, and then a

"limma" differential analysis was performed between the two subgroups. A total of 144 differential mRNA were obtained, including 116 upregulated mRNA, and 28 downregulated mRNA. GPX2 mRNA was strongly expressed in the high *NMRAL2P* expression group and the difference multiple was the largest in this group (logFC =3.17; $p < 0.001$; Fig. 6A). The expression of GPX2 increased when *NMRAL2P-oe* was transferred into TU177 and AMC-HN-8 cells and the expression of GPX2 decreased when *NMRAL2P* was knocked down (Figs. 6B, 6C). Previous studies have shown that Nrf2 is the transcription factor of GPX2 (*Baird & Yamamoto, 2020*; *Li, Jiang & Wu, 2020*). QRT-PCR was used to verify the effectiveness of Nrf2's overexpression (Fig. 6D) and to confirm shNrf2 construction. The expression of Nrf2 was over 40% lower compared to the vector (Fig. 6E). The expression of GPX2 increased or decreased, respectively, when Nrf2-oe and shNrf2 were transferred into TU177 and AMC-HN-8 cells (Figs. 6F, 6G), indicating that Nrf2 acts upstream of *NMRAL2P*. The relative expression of *NMRAL2P* and Nrf2 was also proportional to the relative expression of GPX2 in the TCGA data set (Figs. 6H, 6I). RIP experiments were carried out in TU177 and AMC-HN-8 with Nrf2 antibody to further investigate the role of *NMRAL2P* in Nrf2's ability to boost the transcription of GPX2. The results showed that *NMRAL2P* was enriched in the Nrf2 antibody group (Fig. 6J), indicating *NMRAL2P* and Nrf2 work in combination. *NMRAL2P*-oe and pcDNA3.1 plasmids were transferred into TU177 cells, and ChIP assay was carried out with a Nrf2 antibody. The GPX2 promoter region (antioxidant response element; ARE; -GTGACTCAGTG-) showed a statistically significant increase in the *NMRAL2P* overexpression group compared with the vector group (Fig. 6K). These findings indicated that *NMRAL2P* can combine with Nrf2 to deliver Nrf2 into the GPX2 promoter region, enhancing the transcription of GPX2.

GPX2 knockdown can reverse the tumor-promoting effect of *NMRAL2P*

Functional recovery assays were performed in order to confirm the contribution of *NMRAL2P* to the operation of GPX2. A GPX2 knockdown plasmid was constructed with greater than 30% efficiency (Figs. 7A, 7B). After knocking down the levels of GPX2 mRNA, the migration, invasion, and proliferation abilities of tumor cells decreased (Fig. S3). *NMRAL2P*-oe was transferred into TU177 and AMC-HN-8 cells and the results showed that the overexpression of *NMRAL2P* enhanced the proliferation, migration, and invasion of tumor cells. However, when shGPX2 was transferred into TU177 and AMC-HN-8 cells, this tumor-promoting effect was diminished (Figs. 7C–7H). ROS and MAD decreased concurrently with the overexpression of *NMRAL2P*, and ROS and MAD essentially returned to normal after GPX2 was downregulated (Figs. 7I, 7J). SOD activity showed the opposite trend. These results demonstrate that GPX2 knockdown can reverse the tumor-promoting effect of *NMRAL2P*. To further verify that the effect of *NMRAL2P* on tumors is the result of oxidative stress, an oxidative stress inhibitor, Tempol, was used to reduce the effect of oxidative stress. The results showed that the decrease in the migration, invasion, and proliferation of head and neck tumor cells caused by GPX2 knockdown was reversed by Tempol (1 mM; Fig. S4).

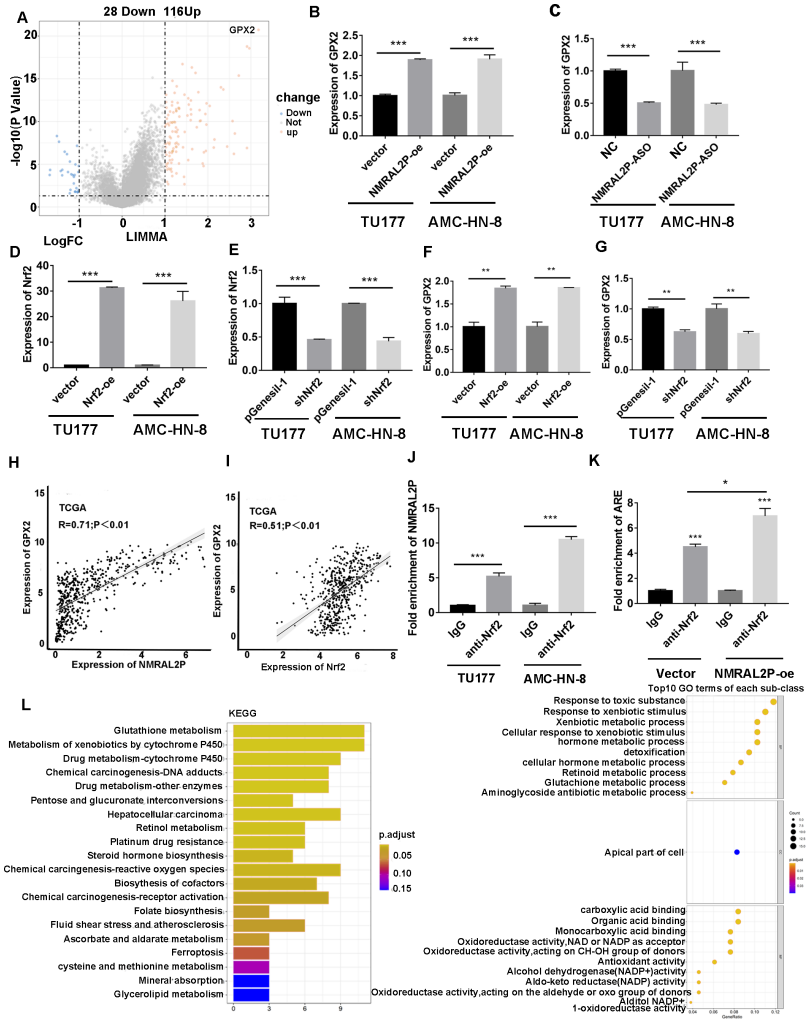

Figure 6 ***NMRAL2P*** **promotes the transcription of GPX2 by binding to Nrf2.** (A) Differential analysis between the high- and low- expression groups of *NMRAL2P* in the TCGA dataset. (B) *NMRAL2P* was overexpressed in TU177 and AMC-HN-8 cells, and GPX2 changes were verified by QRT-PCR. (C) *NMRAL2P*-ASO was transfected into TU177 and AMC-HN-8 cells and the change of GPX2 was verified by QRT-PCR. (D–E) Verification of overexpression and knockdown efficiency of Nrf2-oe and shNrf2 in TU177 and AMC-HN-8 cells by QRT-PCR, respectively. (F–G) To verify the changes of GPX2 after overexpression or knockdown of Nrf2 in TU177 and AMC-HN-8 cells by QRT-PCR, respectively. (H) The relative expression of *NMRAL2P* is proportional to the relative expression of *GPX2*. (I) The relative expression of Nrf2 is proportional to the relative expression of GPX2. (J) The relationship between *NMRAL2P* and Nrf2, verified by RIP assay. (K) *NMRAL2P* overexpression increases the amount of the Nrf2 binding GPX2 promoter region (ARE, Antioxidant response element, (-GTGACTCAGTG-)). (L) The pathway of enrichment of differentially expressed genes in *NMRAL2P* high and low expression groups. (KEGG, Kyoto Encyclopedia of Genes and Genomes; GO, Gene Ontology).

Full-size DOI: 10.7717/peerj.16140/fig-6

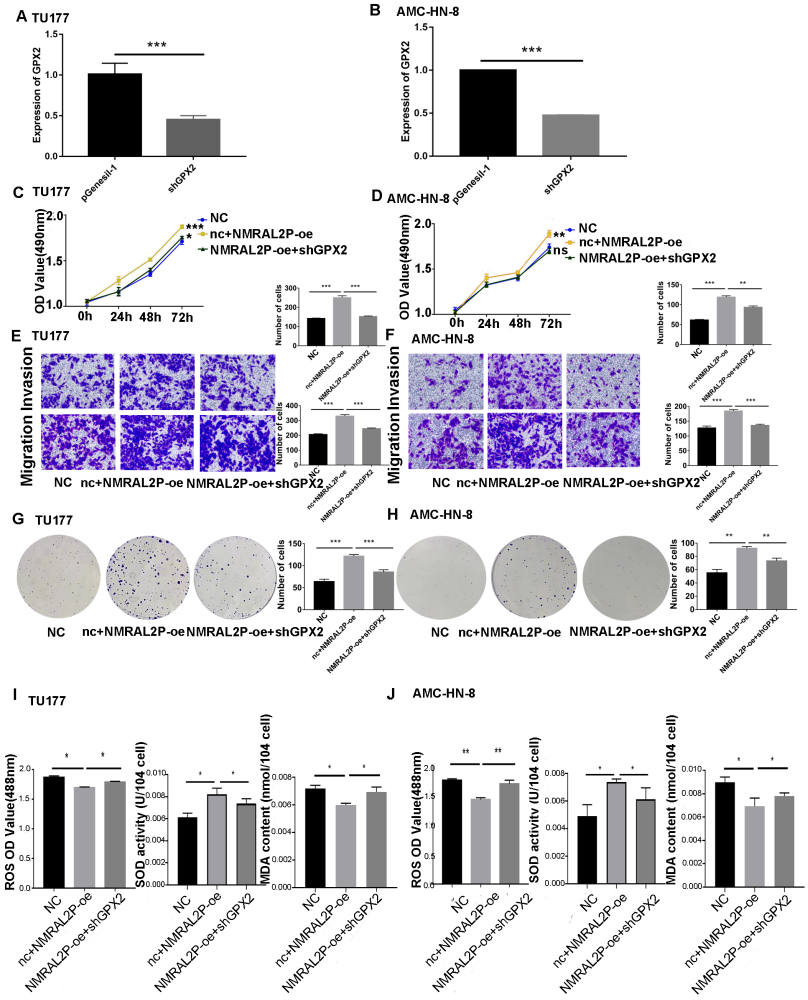

Figure 7 ***NMRAL2P* plays a role in promoting cancer through ENO1.** (A–B) Verification of shGPX2 knockdown efficiency in TU177 and AMC-HN-8 cells by QRT-PCR. (C–H) MTS, Transwell, and colony formation demonstrated that knockdown of GPX2 partially attenuated the enhanced cell proliferation, migration, and invasion induced by overexpression of *NMRAL2P* in TU177 and AMC-HN-8 cells. (I–J) In TU177 and AMC-HN-8 cells, the knockout part of GPX2 gene enhanced the reduction of oxidative stress caused by *NMRAL2P* overexpression. (NC: pcDNA3.1 + pGenesil-1, nc + NMRAL2P-oe: pGenesil-1 + NMRAL2P-oe).

Full-size DOI: 10.7717/peerj.16140/fig-7

NMRAL2P overexpression enriches the ROS-related pathways

DE mRNA were identified by dividing *NMRAL2P* into a high and a low expression group based on the median. KEGG and GO enrichment analyses were then used to examine the identified DE mRNA. The KEGG enrichment analysis identified the processes that were enriched in the DE mRNA, including glutathione metabolism, pentose and glucuronate interconversions, and chemical carcinogenesis-reactive oxygen species. The GO enrichment analysis identified the following pathways: response to a toxic chemical,

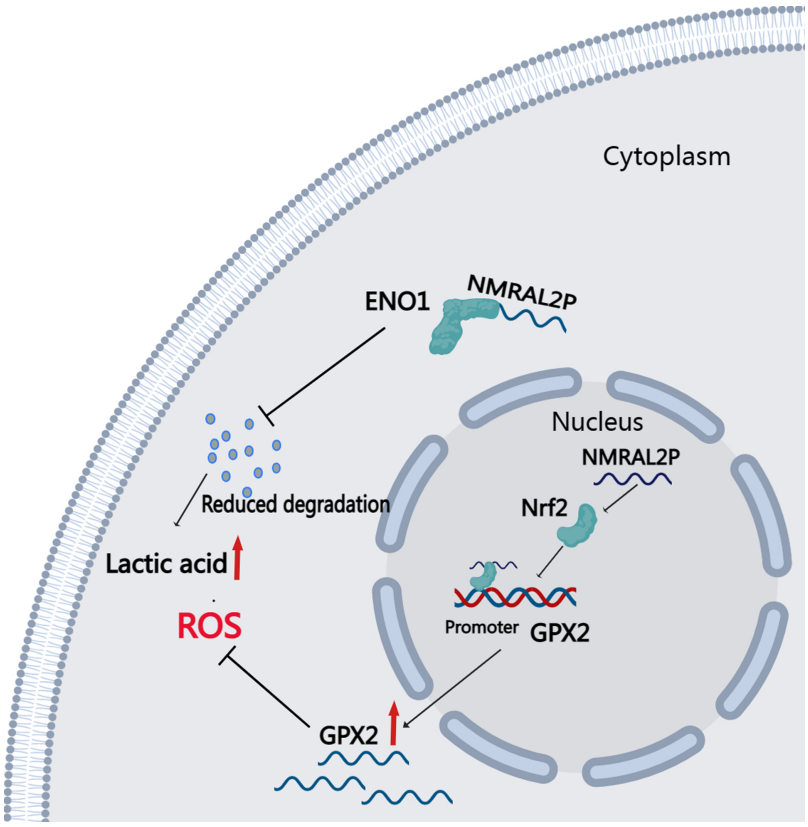

Figure 8 **Downstream Mechanism Diagram of *NMRAL2P*.**
Full-size DOI: 10.7717/peerj.16140/fig-8

response to a xenobiotic stimulus, and response to a metabolic activity (Fig. 6L). The mechanism diagram is shown in Fig. 8.

DISCUSSION

This study identified 16 DE lncRNA related to oxidative stress through differential and correlation analyses of 546 head and neck cancers from TCGA. The differential expression and effect of these 16 DE lncRNA on prognosis was verified using samples from the library of the Second Hospital of Hebei Medical University. Only *NMRAL2P* was substantially expressed in cancer tissues and predicted a poor prognosis. *NMRAL2P* is primarily found in the nucleus. Functional assays *in vitro* show that *NMRAL2P* promotes the migration and proliferation of head and neck tumor cells, promotes lactic acid and SOD, and reduces ROS and MAD production. Western blot assays and further mass spectrometry analysis confirmed that *NMRAL2P* bound to protein ENO1 and prevented ENO1 from degrading. In the group with high *NMRAL2P* expression, the expression level of GPX2 was higher, and the difference multiple was the highest. Further assays confirmed that *NMRAL2P* promotes the transcription of GPX2 by binding to Nrf2. These results indicate that *NMRAL2P* can: promote the occurrence of glycolysis by binding to protein ENO1, provide tumor cells with energy, and subsequently promote tumor cell migration, invasion, and immune escape. By

acting on GPX2 and scavenging excessive oxygen free radicals, *NMRAL2P* can also shield tumor cells from oxidative injury.

ENO1 (enolase), also referred to as 2-phosphate-D-glycerol hydrolase, is an essential enzyme in the glycolysis process as it catalyzes the transformation of 2-phosphate-glyceric acid into phosphoenolpyruvate. ENO1 has been shown to be highly expressed in tissue samples from a variety of tumor types (*Huang et al., 2022b*; *Gou et al., 2021*; *Hou et al., 2021*). High ENO1 expression predicts poor prognosis in patients with liver cancer and lung cancer and also indicates more severe tumor type and later stage tumors (*Zhang, Lu & Yang, 2020*; *Zhang, Wang & Dong, 2018*). Breast cancer lymphatic metastasis and ENO1 are also linked (*Alagundagi et al., 2023*). ENO1 can increase the process of glycolysis, help prevent immune cell destruction and the role of growth inhibitors in tumors (*Hsiao et al., 2013*), promote the growth of tumor blood vessels, provide more nutrients to cells, promote tumor growth and migration (*Huang et al., 2022a*), promote malignant proliferation, and act on tumor-related pathways (*Hua et al., 2021*). The increased expression of ENO1 in all malignancies signifies the heightened potential of migration and invasion, which relies on the type of tumor and the subcellular localization of ENO1 (*Ejeskär et al., 2005*). In this study, ENO1 was abundantly expressed in cancer tissues and was correlated with poor prognosis. The cancer-promoting effect of *NMRAL2P* can be weakened by ENO1 knockdown. These results indicate *NMRAL2P* plays a cancer promoting role, promoting glycolysis by binding to the ENO1 protein.

Glycolysis activation also produces a significant amount of ROS, resulting in the disruption of the oxidant/reductant balance, leading to DNA and protein damage, and ultimately cell death (*Lan et al., 2020*). By promoting the production of reducing agents, tumor cells can lessen the harm caused by oxidants such as ROS. It is well known that GPX2 is a significant reductant in tumor tissues and is substantially expressed in various malignancies (*Esworthy, Doroshow & Chu, 2022*; *Yang et al., 2022*). GPX2 can promote the migration and invasion of prostate, pancreatic, and ovarian cancer cells through the Wnt/β-catenin/EMT pathway (*Li, Dai & Niu, 2020*; *Wang et al., 2019*; *Zhang et al., 2018*). This study also confirmed that *NMRAL2P* can promote the transcription of GPX2 and neutralize excessive ROS. GPX2, NQO1, and HO-1 are downstream of Nrf2 (*Rojodela Vega, Chapman & Zhang, 2018*).

The effect of Nrf2 on several genes in tumor cells is mostly related to the removal of oxidants and the restoration of the oxidation/reduction balance in these cells. Nrf2 binds to Keap1 when oxidative stress is not present. When oxidative stress is triggered, Nrf2 is released from Keap1 and transferred into the nucleus, where it promotes the transcription of genes related to oxidative stress, neutralizing ROS by generating a large number of genes that reduce ROS, thus keeping the body's oxidation and reduction levels balanced (*Kansanen et al., 2013*). In addition to directly promoting the transcription of related mRNA, *Nrf2* can also promote the transcription of long noncoding RNAs such *LUCAT1, ODRUL, RoR*, and *TUG1* (*Luzón-Toro et al., 2019*; *Gao et al., 2017*; *Zhang et al., 2014*; *Yang et al., 2020*). Prior research has also confirmed that *NMRAL2P* is downstream of Nrf2 and can promote the transcription of NQO1 and neutralize excess oxidants. Nrf2 is not only the main gene for oxidative stress (*Johnson et al., 2017*;

Bhattacharjee, Li & Dashwood, 2020), but it can also act on p53 and prevent apoptosis (*Puca et al., 2009*). In addition, it can act on the wtp53 factor, have a carcinogenic role, and promote the immunological escape of tumor cells (*Aubrey et al., 2018*). This study confirmed that *NMRAL2P* can boost Nrf2's role in promoting the transcription of GPX2.

CONCLUSION

The purpose of this study was to analyze the role of lncRNA related with oxidative stress in head and neck tumors. High expression of *NMRAL2P* in head and neck malignancies predicted poor prognosis. Functional experiments showed that *NMRAL2P* can promote the production of lactic acid and SOD, reduce the production of ROS and MDA, and increase the invasion and migration abilities of head and neck tumor cells. The cytoplasmic portion of *NMRAL2P* can bind to the ENO1 protein, postpone ENO1's breakdown, promote glycolysis, and provide extra energy to tumor cells. The gene can also boost Nrf2's role in promoting the transcription of GPX2, neutralize excessive oxidation production, and prevent tumor cells from being destroyed by oxidants.

ACKNOWLEDGEMENTS

The authors are grateful to Prof. Wang Baoshan for guidance on the design of this study.

ADDITIONAL INFORMATION AND DECLARATIONS

Funding

This work was supported by the Project of the National Natural Science Foundation of China (Study on the mechanism of epigenetic regulation of SOCS1 and ATF3 expression by DNA hypomethylation activated LINC00668 in promoter region to promote invasion and metastasis of laryngeal squamous cell carcinoma: 81972553). The funders had no role in study design, data collection and analysis, decision to publish, or preparation of the manuscript.

Grant Disclosures

The following grant information was disclosed by the authors:
National Natural Science Foundation of China: 81972553.

Competing Interests

The authors declare there are no competing interests.

Author Contributions

- Qian Nie performed the experiments, analyzed the data, authored or reviewed drafts of the article, and approved the final draft.
- Huan Cao analyzed the data, authored or reviewed drafts of the article, and approved the final draft.
- JianWang Yang performed the experiments, prepared figures and/or tables, and approved the final draft.

- Tao Liu performed the experiments, prepared figures and/or tables, and approved the final draft.
- BaoShan Wang conceived and designed the experiments, prepared figures and/or tables, authored or reviewed drafts of the article, and approved the final draft.

Human Ethics

The following information was supplied relating to ethical approvals (i.e., approving body and any reference numbers):

The informed consent and the consent procedure gained approval from the Research Ethics Committee of the second hospital of Hebei Medical University(Ethical Application Ref:2021-R012-01)

Data Availability

The following information was supplied regarding data availability:

The raw data, including Western blots, are available at Figshare:

Nie, Qian (2023). Raw data , western blot and code.zip. figshare. Dataset. https://doi.org/10.6084/m9.figshare.22678120.v1

The code and additional raw data are available in the Supplemental Files.

Supplemental Information

Supplemental information for this article can be found online at http://dx.doi.org/10.7717/peerj.16140#supplemental-information.

REFERENCES

Alagundagi DB, Ghate SD, Rajendra VKJ, Gollapalli P, Shetty VV, D'Souza C, Shetty P, Patil P. 2023. Exploring breast cancer exosomes for novel biomarkers of potential diagnostic and prognostic importance. *3 Biotech* **13**:7 DOI 10.1007/s13205-022-03422-w.

Aubrey BJ, Kelly GL, Janic A, Herold MJ, Strasser A. 2018. How does p53 induce apoptosis and how does this relate to p53-mediated tumour suppression? *Cell Death and Differentiation* **25**:104–113 DOI 10.1038/cdd.2017.169.

Baird L, Yamamoto M. 2020. The molecular mechanisms regulating the KEAP1-NRF2 pathway. *Molecular and Cellular Biology* **40**:e00099-20 DOI 10.1128/MCB.00099-20.

Bhattacharjee S, Li J, Dashwood RH. 2020. Emerging crosstalk between long non-coding RNAs and Nrf2 signaling. *Cancer Letters* **490**:154–164 DOI 10.1016/j.canlet.2020.07.011.

Chen L, Huang L, Gu Y, Cang W, Sun P, Xiang Y. 2022. Lactate-lactylation hands between metabolic reprogramming and immunosuppression. *International Journal of Molecular Sciences* **23**:11943 DOI 10.3390/ijms231911943.

Chen P, Wei F, Li R, Li ZQ, Kashif MH, Zhou RY. 2019. Comparative acetylomic analysis reveals differentially acetylated proteins regulating anther and pollen development in kenaf cytoplasmic male sterility line. *Physiologia Plantarum* **166**:960–978 DOI 10.1111/ppl.12850.

Chen L, Zhong Y, Yang X, Zhang Q, Wu X. 2021. Downregulation of GTSE1 leads to the inhibition of proliferation, migration, and Warburg effect in cervical cancer by blocking LHDA expression. *Journal of Obstetrics and Gynaecology Research* **47**:3913–3922 DOI 10.1111/jog.15000.

De Berardinis RJ, Lum JJ, Hatzivassiliou G, Thompson CB. 2008. The biology of cancer: metabolic reprogramming fuels cell growth and proliferation. *Cell Metabolism* **7**:11–20 DOI 10.1016/j.cmet.2007.10.002.

Ejeskär K, Krona C, Carén H, Zaibak F, Li L, Martinsson T, Ioannou PA. 2005. Introduction of in vitro transcribed ENO1 mRNA into neuroblastoma cells induces cell death. *BMC Cancer* **5**:161 DOI 10.1186/1471-2407-5-161.

Esworthy RS, Doroshow JH, Chu FF. 2022. The beginning of GPX2 and 30 years later. *Free Radical Biology and Medicine* **188**:419–433 DOI 10.1016/j.freeradbiomed.2022.06.232.

Gao M, Zhao B, Chen M, Liu Y, Xu M, Wang Z, Liu S, Zhang C. 2017. Nrf-2-driven long noncoding RNA ODRUL contributes to modulating silver nanoparticle-induced effects on erythroid cells. *Biomaterials* **130**:14–27 DOI 10.1016/j.biomaterials.2017.03.027.

Ginckels P, Holvoet P. 2022. Oxidative stress and inflammation in cardiovascular diseases and cancer: role of non-coding RNAs. *Yale Journal of Biology and Medicine* **95**:129–152.

Gou Y, Li F, Huo X, Hao C, Yang X, Pei Y, Li N, Liu H, Zhu B. 2021. ENO1 monoclonal antibody inhibits invasion, proliferation and clone formation of cervical cancer cells. *American Journal of Cancer Research* **11**:1946–1961.

Hou JY, Cao J, Gao LJ, Zhang FP, Shen J, Zhou L, Shi JY, Feng YL, Yan Z, Wang DP, Cao JM. 2021. Upregulation of α enolase (ENO1) crotonylation in colorectal cancer and its promoting effect on cancer cell metastasis. *Biochemical and Biophysical Research Communications* **578**:77–83 DOI 10.1016/j.bbrc.2021.09.027.

Hsiao KC, Shih NY, Fang HL, Huang TS, Kuo CC, Chu PY, Hung YM, Chou SW, Yang YY, Chang GC, Liu KJ. 2013. Surface α-enolase promotes extracellular matrix degradation and tumor metastasis and represents a new therapeutic target. *PLOS ONE* **8**:e69354 DOI 10.1371/journal.pone.0069354.

Hsu PP, Sabatini DM. 2008. Cancer cell metabolism: Warburg and beyond. *Cell* **134**:703–707 DOI 10.1016/j.cell.2008.08.021.

Hua Q, Wang D, Zhao L, Hong Z, Ni K, Shi Y, Liu Z, Mi B. 2021. AL355338 acts as an oncogenic lncRNA by interacting with protein ENO1 to regulate EGFR/AKT pathway in NSCLC. *Cancer Cell International* **21**:525 DOI 10.1186/s12935-021-02232-z.

Huang CK, Sun Y, Lv L, Ping Y. 2022a. ENO1 and cancer. *Molecular Therapy—Oncolytics* **24**:288–298 DOI 10.1016/j.omto.2021.12.026.

Huang Z, Yan Y, Wang T, Wang Z, Cai J, Cao X, Yang C, Zhang F, Wu G, Shen B. 2022b. Identification of ENO1 as a prognostic biomarker and molecular target among ENOs in bladder cancer. *Journal of Translational Medicine* **20**:315 DOI 10.1186/s12967-022-03509-1.

Johnson GS, Li J, Beaver LM, Dashwood WM, Sun D, Rajendran P, Williams DE, Ho E, Dashwood RH. 2017. A functional pseudogene, NMRAL2P, is regulated by Nrf2 and serves as a coactivator of NQO1 in sulforaphane-treated colon cancer cells. *Molecular Nutrition & Food Research* **61**:10 DOI 10.1002/mnfr.201600769.

Kansanen E, Kuosmanen SM, Leinonen H, Levonen AL. 2013. The Keap1-Nrf2 pathway: mechanisms of activation and dysregulation in cancer. *Redox Biology* **1**:45–49 DOI 10.1016/j.redox.2012.10.001.

Lan Z, Yao X, Sun K, Li A, Liu S, Wang X. 2020. The interaction between lncRNA SNHG6 and hnRNPA1 contributes to the growth of colorectal cancer by enhancing aerobic glycolysis through the regulation of alternative splicing of PKM. *Frontiers in Oncology* **10**:363 DOI 10.3389/fonc.2020.00363.

Li F, Dai L, Niu J. 2020. GPX2 silencing relieves epithelial-mesenchymal transition, invasion, and metastasis in pancreatic cancer by downregulating Wnt pathway. *Journal of Cellular Physiology* **235**:7780–7790 DOI 10.1002/jcp.29391.

Li T, Jiang D, Wu K. 2020. p62 promotes bladder cancer cell growth by activating KEAP1/NRF2-dependent antioxidative response. *Cancer Science* **111**:1156–1164 DOI 10.1111/cas.14321.

Lin X, Dinglin X, Cao S, Zheng S, Wu C, Chen W, Li Q, Hu Q, Zheng F, Wu Z, Lin DC, Yao Y, Xu X, Xie Z, Liu Q, Yao H, Hu H. 2020. Enhancer-driven lncRNA BDNF-AS induces endocrine resistance and malignant progression of breast cancer through the RNH1/TRIM21/mTOR cascade. *Cell Reports* **31**:107753 DOI 10.1016/j.celrep.2020.107753.

Luo Y, Wang Q, Teng L, Zhang J, Song J, Bo W, Liu D, He Y, Tan A. 2020. LncRNA DANCR promotes proliferation and metastasis in pancreatic cancer by regulating miRNA-33b. *FEBS Open Bio* **10**:18–27 DOI 10.1002/2211-5463.12732.

Luzón-Toro B, Fernández RM, Martos-Martínez JM, Rubio-Manzanares-Dorado M, Antiñolo G, Borrego S. 2019. LncRNA LUCAT1 as a novel prognostic biomarker for patients with papillary thyroid cancer. *Scientific Reports* **9**:14374 DOI 10.1038/s41598-019-50913-7.

Matsui A, Ikeda T, Enomoto K, Hosoda K, Nakashima H, Omae K, Watanabe M, Hibi T, Kitajima M. 2000. Increased formation of oxidative DNA damage, 8-hydroxy-2'-deoxyguanosine, in human breast cancer tissue and its relationship to GSTP1 and COMT genotypes. *Cancer Letters* **151**:87–95 DOI 10.1016/s0304-3835(99)00424-3.

Park E, Chung SW. 2019. ROS-mediated autophagy increases intracellular iron levels and ferroptosis by ferritin and transferrin receptor regulation. *Cell Death & Disease* **10**:822 DOI 10.1038/s41419-019-2064-5.

Pascale RM, Calvisi DF, Simile MM, Feo CF, Feo F. 2020. The Warburg effect 97 years after its discovery. *Cancers (Basel)* **12**:2819 DOI 10.3390/cancers12102819.

Puca R, Nardinocchi L, Sacchi A, Rechavi G, Givol D, D'Orazi G. 2009. HIPK2 modulates p53 activity towards pro-apoptotic transcription. *Molecular Cancer* **8**:85 DOI 10.1186/1476-4598-8-85.

R Core Team. 2021. R: a language and environment for statistical computing. Version 4.1.2. Vienna: R Foundation for Statistical Computing. *Available at https://www.r-project.org*.

Rojodela Vega M, Chapman E, Zhang DD. 2018. NRF2 and the hallmarks of cancer. *Cancer Cell* **34**:21–43 DOI 10.1016/j.ccell.2018.03.022.

Safran M, Dalah I, Alexander J, Rosen N, Iny Stein T, Shmoish M, Nativ N, Bahir I, Doniger T, Krug H, Sirota-Madi A, Olender T, Golan Y, Stelzer G, Harel A, Lancet D. 2010. GeneCards version 3: the human gene integrator. *Database (Oxford)* **2010**:baq020 DOI 10.1093/database/baq020.

Tan YT, Lin JF, Li T, Li JJ, Xu RH, Ju HQ. 2021. LncRNA-mediated posttranslational modifications and reprogramming of energy metabolism in cancer. *Cancer Communications (Lond)* **41**:109–120 DOI 10.1002/cac2.12108.

Tian J, Lou J, Cai Y, Rao M, Lu Z, Zhu Y, Zou D, Peng X, Wang H, Zhang M, Niu S, Li Y, Zhong R, Chang J, Miao X. 2020. Risk SNP-mediated enhancer-promoter interaction drives colorectal cancer through both *FADS2* and *AP002754.2*. *Cancer Research* **80**:1804–1818 DOI 10.1158/0008-5472.CAN-19-2389.

Tomczak K, Czerwińska P, Wiznerowicz M. 2015. The cancer genome atlas (TCGA): an immeasurable source of knowledge. *Contemporary Oncology* **19**:A68–A77 DOI 10.5114/wo.2014.47136.

Wang Y, Cao P, Alshwmi M, Jiang N, Xiao Z, Jiang F, Gu J, Wang X, Sun X, Li S. 2019. GPX2 suppression of H_2O_2 stress regulates cervical cancer metastasis and apoptosis via activation of the β-catenin-WNT pathway. *OncoTargets and Therapy* **12**:6639–6651 DOI 10.2147/OTT.S208781.

Xiao H, Wang J, Yan W, Cui Y, Chen Z, Gao X, Wen X, Chen J. 2018. GLUT1 regulates cell glycolysis and proliferation in prostate cancer. *Prostate* **78**:86–94 DOI 10.1002/pros.23448.

Yang G, Yin H, Lin F, Gao S, Zhan K, Tong H, Tang X, Pan Q, Gou X. 2020. Long noncoding RNA TUG1 regulates prostate cancer cell proliferation, invasion and migration via the Nrf2 signaling axis. *Pathology, Research and Practice* **216**:152851 DOI 10.1016/j.prp.2020.152851.

Yang M, Zhu X, Shen Y, He Q, Qin Y, Shao Y, Yuan L, Ye H. 2022. GPX2 predicts recurrence-free survival and triggers the Wnt/β-catenin/EMT pathway in prostate cancer. *PeerJ* **10**:e14263 DOI 10.7717/peerj.14263.

Zhang L, Lu T, Yang Y. 2020. α-enolase is highly expressed in liver cancer and promotes cancer cell invasion and metastasis. *Oncology Letters* **20**:152 DOI 10.3892/ol.2020.12003.

Zhang G, Sun J, Zhang X. 2022. A novel Cuproptosis-related LncRNA signature to predict prognosis in hepatocellular carcinoma. *Scientific Reports* **12**:11325 DOI 10.1038/s41598-022-15251-1.

Zhang L, Wang H, Dong X. 2018. Diagnostic value of α-enolase expression and serum α-enolase autoantibody levels in lung cancer. *Jornal Brasileiro de Pneumologia* **44**:18–23 DOI 10.1590/S1806-37562016000000241.

Zhang Z, Qu J, Zheng C, Zhang P, Zhou W, Cui W, Mo X, Li L, Xu L, Gao J. 2018. Nrf2 antioxidant pathway suppresses Numb-mediated epithelial-mesenchymal transition during pulmonary fibrosis. *Cell Death & Disease* **9**:83 DOI 10.1038/s41419-017-0198-x.

Zhang Y, Xia J, Li Q, Yao Y, Eades G, Gernapudi R, Duru N, Kensler TW, Zhou Q. 2014. NRF2/long noncoding RNA ROR signaling regulates mammary stem cell expansion and protects against estrogen genotoxicity. *Journal of Biological Chemistry* **289**:31310–31318 DOI 10.1074/jbc.M114.604868.